ECT* PREPRINT

Self–energy of Λ in finite nuclei

M. Hjorth–Jensen[a], A. Polls[b], A. Ramos[b] and H. Müther[c]

[a]ECT*, European Centre for Theoretical Studies in Nuclear Physics and Related Areas, Trento, Italy

[c]Institut für Theoretische Physik, Universität Tübingen, Tübingen, Germany

[b] Departament d'Estructura i Constituents de la Materia, Universitat de Barcelona, Barcelona, Spain

[c]Institut für Theoretische Physik, Universität Tübingen, Tübingen, Germany

ECT* preprint #: ECT*–96–008

Self-energy of Λ in finite nuclei

M. Hjorth–Jensen

ECT*, European Centre for Studies in Theoretical Nuclear Physics and Related Areas, Trento, Italy

A. Polls and A. Ramos

Departament d'Estructura i Constituents de la Matèria, Universitat de Barcelona, Barcelona, Spain

H. Müther

Institut für Theoretische Physik, Universität Tübingen, Tübingen, Germany

The self–energy of the strange baryon Λ in ^{17}O is calculated using a microscopic many–body approach which accounts for correlations beyond the mean–field or Hartree–Fock approximation. The non-locality and energy-dependence of the Λ self–energy is discussed and the effects on the bound and scattering states are investigated. For the nucleon–hyperon interaction, we use the potential models of the Jülich and Nijmegen groups.

I. INTRODUCTION

Hypernuclear physics has received a lot of attention since the early emulsion and bubble chamber experiments [1] aimed at establishing how the presence of a new flavor (strangeness) broadens the knowledge achieved by the conventional field of nuclear physics and helps in understanding the breaking of SU(3) symmetry. Although major achievements in hypernuclear physics have been taken at a very slow pace due to limited statistics, the in–flight (K^-, π^-) counter experiments carried out at CERN [2,3] and Brookhaven [4] revealed a considerable amount of hypernuclear features, such as small spin–orbit strength, increased validity of single–particle motion of the Λ, narrow widths of Σ–hypernuclei, etc, injecting a renewed interest in the field. Since then, the experimental facilities have been upgraded and experiments using the (π^+, K^+) and $(K^-_{\text{stopped}}, \pi^0)$ reactions are being conducted at the Brookhaven AGS and KEK accelerators with higher beam intensities and improved energy resolution. Moreover, the photo– and electro–production of strangeness will be studied at CEBAF [5]. It is expected that the new improved experimental data will bring the field of hypernuclear physics to a stage in which major advances can be made.

From the theoretical side, one of the goals of hypernuclear research is to relate the hypernuclear observables to the bare hyperon-nucleon (YN) interaction. The experimental difficulties associated to the short lifetime of hyperons and low intensity beam fluxes have limited the number of ΛN and ΣN scattering events to less than one thousand [6–10], not being enough to fully constrain the YN interaction. At present, there are two meson-exchange YN potentials: that of the Nijmegen group [11], where the corresponding baryon–baryon-meson vertices are subject to strict SU(3) symmetry, and that of the Jülich group [12], which assumes a stronger SU(6) symmetry and therefore all the coupling constants at the strange vertices can be related to the NN coupling constants. Although both models are able to describe the YN scattering data, their spin–isospin structure is very different. Therefore, more data on YN scattering, especially the measurement of spin observables, are highly desirable. In the lack of such data, alternative information can be obtained from the study of hypernuclei. One possibility is to focus on light hypernuclei, such as $^3_\Lambda$He, $^3_\Lambda$H and $^4_\Lambda$He, which can be treated "exactly" solving 3-body Faddeev [14,15] and 4-body Yakubovsky [16] equations. However, the power of these techniques is limited by the scarce amount of spectroscopic data. Only the ground state energies and a particle–stable excited state for each A=4 species can be used to put further constraints on the YN interaction. Another possibility is the study of hypernuclei with larger masses. They can be reasonably well described by a shell–model picture and, on the other hand, provide a substantial amount of hypernuclear excited states. Obtaining spectroscopic data at high resolution is one of the ultimate goals of the hypernuclear program at CEBAF. Hypernuclear structure calculations must be performed with an effective YN interaction (G–matrix) obtained from the free YN potential by solving a Bethe–Goldstone equation. The comparison with data will help to elucidate which pieces of of the bare YN potential need to be changed for a better agreement with experiment. Some shell–model calculations have already been performed using a nuclear matter YN G–matrix [17,18] or a G–matrix calculated directly in finite nuclei [19,20]. It has been observed that the various potentials predict a quite different positioning of the excited energy levels, showing the suitability of this approach as a tool to constrain the YN interaction.

The aim of this work is to study the self-energy of the Λ in $^{17}_\Lambda$O using a microscopic many–body approach. Our starting point is a nuclear matter G–matrix at a fixed energy and density, which is used to calculate the G–matrix for the finite nucleus including corrections up to second order. This second–order correction, which assumes harmonic oscillator states for the occupied (hole) states and plane waves for the intermediate unbound particle states, incorporates the correct energy and density dependence of the G–matrix. The hypernuclear structure calculations of Ref. [18] take the

nuclear matter G–matrix at the Fermi momentum k_F (density) that reproduces the binding energy of the Λ in the hypernucleus under study. Our second order finite nucleus calculation eliminates the need to choose such an effective Fermi momentum for each single-particle state and hypernucleus. In this sense it is comparable with the finite nucleus calculations of Refs. [19] and [20].

Using this G–matrix we determine a self–energy for the Λ, which is non–local and depends on the energy of the hyperon. Solving the Schrödinger equation with this self–energy we are able to determine the single particle energies and wave functions of the bound hyperon. Our approach also provides automatically the real and imaginary part of the hyperon optical potential at positive energies and, therefore, allows to study the hyperon–nucleus scattering properties. Because of the large momentum transfer, the (γ, K^+) reaction at CEBAF [21] and (π^+, K^+) reaction at KEK [22] give rise to a significant quasifree production, i.e. hyperons in the continuum. The hyperon may then scatter from nucleons or nuclei composing the target material. It is then clear that, in order to analyze such data, a knowledge of the hyperon–nucleus optical potential will be useful and, at present, very few calculations exist. In Ref. [23], an energy dependent local Λ-nucleus potential is calculated from a nuclear matter G–matrix by applying a finite range Local Density Approximation. The hyperon–nucleus optical potential has also been derived from the nucleon–nucleus potential using Dirac phenomenology and symmetry considerations to relate the coupling constants in the strange sector to the non-strange ones [24].

In Section 2 we outline our method to calculate the self–energy of the Λ in a finite nucleus and discuss how it is used in a Schrödinger equation to derive the corresponding eigenvalues and single–particle properties. Our results are presented in Section 3 with a special emphasis on the discussion of the non-locality and energy-dependence of the Λ self–energy. Some concluding remarks are given in Section 4.

II. COMPUTATIONAL DETAILS

A. Evaluation of the Λ self-energy

The self–energy of the Λ is evaluated including the diagrams displayed in Fig. 1. The wiggly interaction lines in this figure refer to a G–matrix approach for the YN interaction in nuclear matter calculated at a fixed baryon density and starting energy. Therefore, as a first step, we calculate this G_{YN}–matrix in a basis for the two-particle states defined in terms of relative and center-of-mass momenta

$$\mathbf{k} = \frac{M_N \mathbf{k_Y} - M_Y \mathbf{k_N}}{M_N + M_Y},$$
$$\mathbf{K} = \mathbf{k_N} + \mathbf{k_Y} ,$$

where M_N is the nucleon mass and M_Y the mass of the hyperon which can be either a Λ (M_Λ) or a Σ (M_Σ). The use of an angle–averaged Pauli operator, see e.g. Ref. [13], allows us to perform a partial wave decomposition. In terms of the quantum numbers of the relative and center–of–mass motion (RCM) the Bethe-Goldstone equation reads

$$
\begin{aligned}
\langle k'l'KL(\mathcal{J})ST_z| \, G_{YN} \, |k''l''KL(\mathcal{J})S'T_z\rangle = \\
\langle k'l'KL(\mathcal{J})ST_z| \, V_{YN} \, |k''l''KL(\mathcal{J})S'T_z\rangle \\
+ \sum_l \sum_{Y=\Lambda\Sigma} \int k^2 dk \, \langle k'l'KL(\mathcal{J})ST_z| \, V_{YN} \, |klKL(\mathcal{J})S'T_z\rangle \\
\times \langle klKL(\mathcal{J})ST_z| \, G_{YN} \, |k''l''KL(\mathcal{J})S'T_z\rangle \\
\times \frac{Q(k,K)}{\omega_{NM} - \frac{K^2}{2(M_N+M_Y)} - \frac{k^2(M_N+M_Y)}{2M_N M_Y} - M_Y + M_\Lambda} \, ,
\end{aligned}
\tag{1}
$$

where Q is the nuclear matter Pauli operator, V_{YN} is the YN potential, and ω_{NM} is the nuclear matter starting energy. The variables k, k', k'' and l, l', l'' denote relative momenta and angular momenta, respectively, while K and L are the quantum numbers of the center-of-mass motion. Further, $\mathcal{J}$, S and T_z represent the total angular momentum, spin and isospin projection, respectively. In our calculations we consider nuclear matter with a Fermi momentum k_F of 1.4 fm^{-1} and a starting energy $\omega_{NM} = -80$ MeV, which is a averaged value for the sum of the single-particle energies of a bound nucleon and a Λ at this density.

Starting from this G_{YN}–matrix in the RCM system, one can obtain the G_{YN}–matrix in the laboratory system through appropriate transformation coefficients [25,26]. With these coefficients, the expression for a two–body wave function

in momentum space using the lab coordinates can be written as [1]

$$
|(k_a l_a j_a t_{z_a})(k_b l_b j_b t_{z_b})JT_z\rangle = \sum_{lL\lambda SJ} \int k^2 dk \int K^2 dK
\begin{Bmatrix} l_a & l_b & \lambda \\ \frac{1}{2} & \frac{1}{2} & S \\ j_a & j_b & J \end{Bmatrix}
$$

$$
\times (-1)^{\lambda+\mathcal{J}-L-S} \hat{\mathcal{J}} \hat{\lambda}^2 \hat{j}_a \hat{j}_b \hat{S}
\begin{Bmatrix} L & l & \lambda \\ S & J & \mathcal{J} \end{Bmatrix}
$$

$$
\times \langle klKL|k_a l_a k_b l_b\rangle \, |klKL(\mathcal{J})SJT_z\rangle ,
$$

(2)

where the term $\langle klKL|k_a l_a k_b l_b\rangle$ is the transformation coefficient from the RCM system to the lab system defined in Refs. [27,28].

Typical matrix elements needed in the calculation are

$$
\langle (k_a l_a j_a t_{z_a})(n_b l_b j_b t_{z_b})JT_z| \, G_{YN} \, |(k_c l_c j_c t_{z_c})(n_d l_d j_d t_{z_d})JT_Z\rangle ,
$$

(3)

for the Hartree–Fock diagram of Fig. 1(a), or

$$
\langle (k_a l_a j_a t_{z_a})(n_b l_b j_b t_{z_b})JT_Z| \, G_{YN} \, |klKL(\mathcal{J})ST_z\rangle ,
$$

(4)

appearing in the second–order diagram of Fig. 1(b). The calculation of these matrix elements require the knowledge of two–body states in a mixed representation with harmonic oscillator (h.o.) and plane wave states given by

$$
|(n_a l_a j_a t_{z_a})(k_b l_b j_b t_{z_b})JT_z\rangle = \int k_a^2 dk_a R_{n_a l_a}(\alpha k_a) \, |(k_a l_a j_a t_{z_a})(k_b l_b j_b t_{z_b})JT_z\rangle ,
$$

(5)

where $k_a l_a j_a$ and $n_a l_a j_a$ are shorthands for plane wave and h.o. functions, respectively, and α is the oscillator parameter which is set to 1.72 fm, a value which is appropriate to describe the single–particle wave functions of the bound nucleons in $^{17}_{\Lambda}$O, the system we are going to discuss. The quantum numbers $l_{a,b}$, $j_{a,b}$ and $t_{z_{a,b}}$ are the single–particle orbital and total angular momenta and isospin projections, respectively. The two–body state is represented by the quantum numbers of the total angular momentum J and isospin projection T_z.

Finally, we are then ready to set up the equations for the various diagrams evaluated in this work. The direct and exchange contributions to the HF approximation, displayed in Fig. 1(a) and (b), yield a real and energy-independent the self-energy. It is given as

$$
\mathcal{V}_{HF}(k_\Lambda k'_\Lambda l_\Lambda j_\Lambda t_{z_\Lambda}) = \frac{1}{\hat{j}_\Lambda^2} \sum_J \sum_{n_h l_h j_h t_{z_h}} \hat{j}^2
$$

$$
\times \langle (k_\Lambda l_\Lambda j_\Lambda t_{z_\Lambda})(n_h l_h j_h t_{z_h})JT_z| \, G_{YN} \, |(k_\Lambda l_\Lambda j_\Lambda t_{z_\Lambda})(n_h l_h j_h t_{z_h})JT_z\rangle ,
$$

(6)

where $\hat{x} = \sqrt{2x+1}$ and $n_h l_h j_h t_{z_h}$ are the quantum numbers of the nucleon hole states. The variables l_Λ, j_Λ, t_{z_Λ} are the orbital angular momentum, total angular momentum and isospin projection ($t_{z_\Lambda} = 0$) of the incoming/outgoing Λ, and k_Λ (k'_Λ) the incoming (outgoing) particle momentum.

To calculate the contributions from the two–particle–one–hole (2p1h) diagrams like the example displayed in Fig. 1 (c) we evaluate the imaginary part first. The real part is obtained through the dispersion relation to be defined below. The analytical expression for the imaginary contribution of the 2p1h diagram, which gives rise to an explicit energy dependence of the self–energy, is

$$
\mathcal{W}_{2p1h}(j_\Lambda l_\Lambda k_\Lambda k'_\Lambda t_{z_\Lambda}\omega) = -\frac{1}{\hat{j}_\Lambda^2} \sum_{n_h l_h j_h t_{z_h}} \sum_J \sum_{lLSJ} \sum_{Y=\Lambda\Sigma} \int k^2 dk \int K^2 dK \hat{J}\hat{T}
$$

$$
\times \langle (k'_\Lambda l_\Lambda j_\Lambda t_{z_\Lambda})(n_h l_h j_h t_{z_h})JT_z| \, G_{YN} \, |klKL(\mathcal{J})SJT_z\rangle
$$

$$
\times \langle klKL(\mathcal{J})SJT_z| \, G_{YN} \, |(k_\Lambda l_\Lambda j_\Lambda t_{z_\Lambda})(n_h l_h j_h t_{z_h})JT_z\rangle
$$

$$
\times \pi\delta\left(\omega + \varepsilon_h - \frac{K^2}{2(M_N+M_Y)} - \frac{k^2(M_N+M_Y)}{2M_N M_Y} - M_Y + M_\Lambda\right) ,
$$

(7)

---

[1]Note the distinction between k_a and k and l_a and l. With the notation k_a or l_a we will refer to the quantum numbers of the single–particle state, whereas l or k without subscripts refer to the coordinates of the relative motion.

where ω is the energy of the Λ measured with respect to the Λ rest mass. The single–hole energies ε_h are set equal to the experimental single-particle energies in ^{16}O. The quantities $klKL(\mathcal{J})SJT_z$ are the quantum numbers of the intermediate YN state. In the above sum over intermediate nucleon and hyperon states, we have to account for the fact that the nucleon particle states should be orthogonal to the hole states. This is done following the local density approximation for the orthogonalization of the intermediate nucleon particle states of Ref. [25].

The contributions to the real part of the self-energy from Eq. (7) can be obtained through the following dispersion relation

$$\mathcal{V}_{2p1h}(j_\Lambda l_\Lambda k_\Lambda k'_\Lambda t_{z_\Lambda}\omega) = \frac{P}{\pi}\int_{-\infty}^{\infty}\frac{\mathcal{W}_{2p1h}(j_\Lambda l_\Lambda k_\Lambda k'_\Lambda t_{z_\Lambda}\omega')}{\omega'-\omega}d\omega', \tag{8}$$

where P means a principal value integral. Since $\mathcal{W}_{2p1h}$ is different from zero only for positive values of ω' and its diagonal matrix elements are negative, this dispersion relation implies that the diagonal elements of $\mathcal{V}_{2p1h}$ will be attractive for negative values of ω. This attraction should increase for small positive energies. It will eventually decrease and become repulsive only for large positive values of the energy of the interacting Λ.

The reader should observe that the Hartree–Fock contribution of Eq. (6) has been obtained with a YN G–matrix calculated in nuclear matter. Therefore, the Hartree–Fock contribution contains already $2p1h$ terms like those displayed in Fig. 1(c), but calculated for nuclear matter. To avoid this double-counting of intermediate YN states, we subtract from the real part of the Λ self-energy a correction term

$$\begin{aligned}
\mathcal{V}_c(j_\Lambda l_\Lambda k_\Lambda k'_\Lambda t_{z_\Lambda}) &= \frac{1}{\hat{j}_\Lambda^{\,2}}\sum_{n_h l_h j_h t_{z_h}}\sum_J\sum_{lLS\mathcal{J}}\sum_{Y=\Lambda\Sigma}\int k^2 dk\int K^2 dK\,\hat{J}\hat{T}\\
&\times \langle(k'_\Lambda l_\Lambda j_\Lambda t_{z_\Lambda})(n_h l_h j_h t_{z_h})JT_z|\,G_{YN}\,|klKL(\mathcal{J})SJT_z\rangle\\
&\times \langle klKL(\mathcal{J})SJT_z|\,G_{YN}\,|(k_\Lambda l_\Lambda j_\Lambda t_{z_\Lambda})(n_h l_h j_h t_{z_h})JT_z\rangle\\
&\times Q(k,K)\left(\omega_{NM}-\frac{K^2}{2(M_N+M_Y)}-\frac{k^2(M_N+M_Y)}{2M_N M_Y}-M_Y+M_\Lambda\right)^{-1},
\end{aligned} \tag{9}$$

where Q is the nuclear matter Pauli operator and ω_{NM} is the nuclear matter starting energy.

In summary, the self–energy of the Λ hyperon reads

$$\Sigma(j_\Lambda l_\Lambda k_\Lambda k'_\Lambda \omega) = V(j_\Lambda l_\Lambda k_\Lambda k'_\Lambda \omega) + iW(j_\Lambda l_\Lambda k_\Lambda k'_\Lambda \omega), \tag{10}$$

with the real part given by

$$V(j_\Lambda l_\Lambda k_\Lambda k'_\Lambda \omega) = \mathcal{V}_{HF}(j_\Lambda l_\Lambda k_\Lambda k'_\Lambda) + \mathcal{V}_{2p1h}(j_\Lambda l_\Lambda k_\Lambda k'_\Lambda \omega) - \mathcal{V}_c(j_\Lambda l_\Lambda k_\Lambda k'_\Lambda) \tag{11}$$

and the imaginary part by

$$W(j_\Lambda l_\Lambda k_\Lambda k'_\Lambda \omega) = \mathcal{W}_{2p1h}(j_\Lambda l_\Lambda k_\Lambda k'_\Lambda \omega). \tag{12}$$

B. Solution of the Schrödinger equation

The self–energy of Eq. (10) can be used as a single–particle potential in a Schrödinger equation in order to investigate bound and scattering states of a Λ in a finite nucleus. The different approximations to the self–energy, i.e. whether we include the $2p1h$ contribution or not, results in different single–particle hamiltonians. The Schrödinger equation is solved by diagonalizing the corresponding single–particle hamiltonian in a complete basis within a spherical box of radius R_{box}. The radius of the box should be larger than the radius of the nucleus considered. The calculated observables are independent of the choice of R_{box}, if it is chosen to be around 15 fm or larger. The method is especially suitable for non–local potentials defined either in coordinate or in momentum space.

A complete and orthonormal set of regular basis functions within this box is given by

$$\Phi_{iljm}(\mathbf{r}) = \langle\mathbf{r}|k_i ljm\rangle = N_{il}j_l(k_i r)\psi_{ljm}(\theta\phi) \tag{13}$$

In this equation ψ_{ljm} represent the spherical harmonics including the spin degrees of freedom and j_l denote the spherical Bessel functions for the discrete momenta k_i which fulfill

$$j_l(k_i R_{box}) = 0. \tag{14}$$

For the specific case of $l = 0$, which we will consider in this paper, the normalization constant is

$$N_{i0} = \frac{i\pi 2^{1/2}}{R_{box}^{3/2}} \; . \tag{15}$$

In this way, the basis functions defined in Eq. (13) are orthogonal and normalized within the box. The single particle hamiltonian for the Λ, consisting out of the kinetic energy and the real part of the self–energy can be evaluated in this basis and the resulting eigenvalue problem

$$\sum_{n=1}^{N_{max}} \langle k_i | \frac{k_i^2}{2m_\Lambda} \delta_{in} + V(\omega = E_\Upsilon) | k_n \rangle \langle k_n | \Upsilon \rangle = E_\Upsilon \langle k_i | \Upsilon \rangle , \tag{16}$$

restricted typically to 20 or 30 states, can be easily solved. Notice that a self–consistent process is performed for each eigenvalue, i.e. the self–energy needs to be evaluated at the energy of the resulting eigenvalue. As a first result, one obtains the negative energies for the bound states and the corresponding wave functions, which are expressed in terms of expansion coefficients for the basis defined in Eq. (13). Furthermore, one also obtains discrete positive energies that correspond to scattering states with radial wave functions which are zero at $r = R_{box}$. Taking into account this fact it is straightforward to evaluate the phase shifts for those energies. Phase shifts for different energies can be obtained by varying R_{box}, see e.g. the discussion in Ref. [25].

III. RESULTS AND DISCUSSION

The results presented in this section have been obtained with two potential models for the free YN–interaction V_{YN}, namely the Nijmegen soft–core potential described in Ref. [11] and the energy independent version with parameter set B of the Jülich group [12,13]. Both potential models are based on meson–exchange theory and include the relevant low–energy mesons. However, contrary to what is the case for the nucleon–nucleon potential, not all parameters which enter the definition of the various potential models, like coupling constants, are left as free parameters to be constrained by the data. The Nijmegen model imposes SU(3) symmetry on the coupling constants leaving the pseudoscalar F/D ratio α as a free parameter adjusted to fit the data ($\alpha = 0.355$). Instead, the Jülich model fixes its value to $\alpha = 2/5$ by imposing the stronger SU(6) symmetry. Thus, various potential models may give different results for various observables.

As an example, we show in Table V the binding energy of the Λ at rest in nuclear matter at saturation density ($k_F = 1.4$ fm^{-1}). These results were obtained using a starting energy $\omega_{NM} = -80$ MeV, which is approximately the sum of the single–particle energies of an average nucleon and a Λ in nuclear matter, and with the center–of–mass momentum of the YN pair at rest. We employ kinetic energies for the single–particle spectrum above the Fermi momentum. The numbers displayed in Table V compare well with the nuclear matter calculations of Reuber *et al.* [13] and Yamamoto *et al.* [18]. One can see that the Nijmegen potential predicts a binding energy for the Λ (–24.35 MeV), which is about 7 MeV weaker than the prediction of the Jülich model (–31.48 MeV). Even larger differences are observed if one inspects the contributions of the various partial waves. While for the case of the Jülich potential the predominant contribution to the binding energy results from the $^3S_1$–$^3D_1$ coupled channel, the largest term for the Nijmegen potential is obtained in the $^1S_0$ channel. In both interaction models a large part of the Λ binding energy is due to the coupling of the ΛN to the ΣN channel. Neglecting this coupling (numbers listed in parenthesis) would result in unbound Λ in the case of the Nijmegen potential.

The main purpose of this work, however, is to study the Λ self–energy in $^{17}_{\Lambda}$O as well as the single–particle properties that can be derived from it. Here we restrict our attention to the states with orbital angular momentum $l_\Lambda = 0$. Unless the comparison turns to be of interest, we will present results for the Jülich interaction only, since it yields the correct Λ binding energy in nuclear matter as obtained when extrapolating from $A \to \infty$ to finite hypernuclei data [29].

We first investigate the properties of the known bound state of an s–wave Λ in $^{17}_{\Lambda}$O. In Table V we display the binding energy, kinetic energy and root–mean–square radius of the Λ obtained by solving the Schrödinger equation for two different choices of the self–energy. As can be seen from this table, both potentials give a bound state already at the Hartree–Fock level. Recall, however, that the label Hartree–Fock approximation here refers to a calculation in terms of the nuclear matter G–matrix. Similar to the case of nuclear matter the Nijmegen potential yields smaller binding energies than the Jülich model also for the finite system. This smaller binding energy predicted by the Nijmegen potential also results in a larger radius for the bound Λ state and a smaller binding energy. This feature can also be seen in Fig. 2, where we plot the corresponding Λ wave functions. For the sake of comparison we also plot the wave function of a $0s_{1/2}$ nucleon in ^{16}O taken from Ref. [26].

The second–order correction introduces additional attraction, which can be understood from the following argument: The total $2p1h$ contribution is given by $\mathcal{V}_{2p1h}$, see Eq. (8), minus the nuclear matter correction term $\mathcal{V}_c$ of Eq. (9). Thus, Eq. (11) introduces the finite nucleus Pauli operator which is less restrictive than the nuclear matter Pauli operator at $k_F = 1.4$ fm^{-1}. Therefore, by allowing for a larger phase space in the sum over intermediate states, the finite nucleus second–order contribution is more attractive than the corresponding nuclear matter result, producing an overall attractive second–order correction. It is important to note that the final result $(HF + 2p1h)$ is stable with respect to the use of different starting energies in the G–matrix. In other words, had we used a different value for the starting energy, ω_{NM}, the HF contribution to the Λ single–particle energy would have had a different value. However, the $2p1h$ contribution would have also been different producing approximately the same final results as shown in Table V.

One of the advantages of the present approach is that it also allows the study of scattering states. Since this is traditionally done in terms of energy–dependent local potentials we now wish to investigate how well our non–local self–energy obtained from Eq. (10) can be represented by a local potential. We start by analyzing the Hartree–Fock contribution, which does not contain any explicit dependence on the energy of the incoming Λ. In this approximation the non–locality arises to some extent from the non–local G interaction but mainly from the Fock exchange term displayed in Fig. 1(b).

The localization of the self–energy is more easily discussed in r–space and therefore it is useful to consider the Fourier–Bessel transform from the momentum space to r–space

$$\mathcal{V}_{HF}(l = 0, r, r') = \frac{2}{\pi} \int k^2 dk \int k'^2 dk' j_0(kr) j_0(k'r') \mathcal{V}_{HF}(l = 0, k, k') \ . \tag{17}$$

We generate a local representation of $\mathcal{V}_{HF}(l = 0, r, r')$ by performing an average of the non–local potential over the coordinate r' weighted with the radial function of the lowest bound state, $\Upsilon_1(r)$

$$\mathcal{V}_{HF}^{loc}(l = 0, r) = \frac{\int dr' r'^2 \mathcal{V}_{HF}(l = 0, r, r') \Upsilon_1(r')}{\Upsilon_1(r)}. \tag{18}$$

This procedure ensures that the local potential $\mathcal{V}_{HF}^{loc}(r)$ will give rise to the same bound state $\Upsilon_1(r)$. Notice that the absence of nodes in the lowest bound state guarantees the numerical stability of this prescription.

The results of this localization are represented by the solid line in Fig. 3. One can see that this local representation might, in first approximation, be characterized by the shape of a Woods–Saxon potential

$$V_{WS}(r) = \frac{V_0}{1 + \exp{(r - R)/a}}, \tag{19}$$

with parameters $V_0 = -22.40$ MeV, $R = 3.15$ fm and $a = 0.6$ fm, shown by the dashed line of Fig. 3. These parameters reproduce the binding energy of the Λ and yield an overlap with the wave function obtained with the Hartree–Fock self–energy equal to 0.99994.

Having established the radial shape of the local effective Λ–nucleus potential for the bound state, we now proceed to study the region of positive energies. By keeping R and a fixed, we allow for an energy dependent depth, $V_0(E)$, chosen to reproduce the same phase shift at each energy as obtained with the non–local Hartree–Fock self–energy. The depth of the Woods–Saxon potential is shown as a function of energy by the dashed line in Fig. 4. The behavior of the Λ–nucleus potential as a function of energy or as a function of the asymptotic momentum k related to this energy, can be characterized by an effective k–mass $m_{k,\Lambda}$ [30]

$$\frac{m_{k,\Lambda}(E, r)}{m_\Lambda} = \left(1 + \frac{m_\Lambda}{k} \frac{dV}{dk}\right)^{-1} = \left(1 + \frac{dV(E, r)}{dE}\right)^{-1}. \tag{20}$$

If we approximate the dashed curve in Fig. 3 by a straight line, we obtain a constant value of this effective mass of about $m_{k,\Lambda}/m_\Lambda = 0.8$. Note that this value is a measure of the momentum dependence or non–locality of the Hartree–Fock self–energy, which is the only source of the effective energy dependence for the local equivalent potential. Beside this effective energy dependence, the second order contribution to the Λ self–energy, $\mathcal{V}_{2p1h}$, also yields an explicit energy dependence, which is tied to the coupling to intermediate $2p1h$ states as shown in Eq. (7). The energy dependence of this dispersive correction can be better visualized by calculating the expectation value of the second order contribution to the self–energy in the $l_\Lambda = 0$ ground state, $\langle \Upsilon_1 \mid \mathcal{V}_{2p1h}(\omega) + i\mathcal{W}_{2p1h}(\omega) \mid \Upsilon_1 \rangle$. In Fig. 5 the real and imaginary parts of the dispersive term of the self–energy are shown as functions of energy. The solid line shows the results obtained with Jülich potential while the dashed line corresponds to the Nijmegen potential. As can be seen from this figure, the absolute value of the imaginary component $\mathcal{W}_{2p1h}$ is slightly larger for the Nijmegen

potential as compared to the Jülich model at small energies ω. Therefore the dispersion relation of Eq. (8) leads to a stronger energy dependence in the real part of the self–energy around $\omega = 0$ in the case of the Nijmegen potential. It is this energy dependence, which leads to the larger $2p1h$ correction for the bound state in the case of the Nijmegen potential (see Table V).

The non–locality of the real part of the complete self–energy (see Eq. (11)) can also be characterized by a local Woods–Saxon with an energy dependent depth, as done with the Hartree–Fock term. The energy dependence of this depth is represented by the solid line of Fig. 4. The difference between the solid and dashed lines is a measure of the non–locality and the explicit energy dependence of the dispersive correction. In the range of energies shown in Fig. 4, the explicit energy dependence should provide attraction increasing with energy, as can be inferred from the real part of the self–energy plotted in Fig. 5. This would imply that the depth V_0 of the local equivalent potential representing the whole self–energy should be more attractive than the one representing the Hartree–Fock approximation. However, due to the non–locality of the second order terms $(\mathcal{V}_{2p1h} - \mathcal{V}_c)$, this attraction can clearly be seen in Fig. 4 only at higher energies. The effective mass characterizing the explicit energy dependence as well as the momentum dependence of the full self–energy can be represented as a product of a k–mass as defined in Eq. (20) and the energy-dependent mass [30]. This total effective mass can be calculated approximately from the depth V_0 of the local equivalent potential by

$$\frac{m_\Lambda^*(E)}{m_\Lambda} = \left(1 - \frac{dV_0(E)}{dE}\right). \tag{21}$$

This effective mass is no longer constant in the range of energies considered in Fig. 4. The value of m^*/m ranges from about 0.7 at low energies to 0.9 at energies above 50 MeV.

The real part of the Λ-nucleus optical potential for $l_\Lambda = 0$ is shown as a function of r in Fig. 6 for several energies of the incoming Λ. Our optical potential exhibits substantial differences with that of Ref. [23] obtained from a nuclear matter G–matrix and the local density approximation employing the Nijmegen model D interaction. The Nijmegen model D gives a nuclear matter Λ binding energy of -40.5 MeV, the attraction being concentrated mainly in the $^3S_1 - ^3D_1$ channel [18]. It is therefore more similar to the potentials of the Jülich group than to the Nijmegen soft-core model. Figure 6 shows that in the energy range $5 - 60$ MeV the depth of our optical potential changes by about 10 MeV, whereas in a similar energy range the depth of the potential obtained in Ref. [23] (see their Fig. 4) varies by about half as much. Moreover, our potential is much shallower. At $\omega = 40$ MeV, for instance, we find a depth of about -9 MeV while a value of -25 MeV is obtained in Ref. [23]. Only part of this attraction (about 5 MeV) can be attributed to the more attractive nuclear matter G–matrix obtained with the Nijmegen D model. Part of the difference can also be attributed to the wider shape of our equivalent Woods–Saxon. We have tried narrower Woods–Saxon potentials that still reproduce reasonably well the binding energy and wave function of the bound state, but the depth at 40 MeV decreased at most by 3 MeV. The remaining difference must be attributed to the different methods used and, therefore, we can conclude that the finite nucleus calculation presented here gives a substantially less attractive optical potential than the local density calculation of Ref. [23].

The imaginary–part of the self-energy $\mathcal{W}_{2p1h}$ as calculated from Eq. (7) is also non–local. To obtain a local representation we follow the same procedure as for the real part shown in Eq. (18). The resulting imaginary part of the Λ–^{16}O optical potential is shown in Fig. 7 for various values of the incoming Λ energy. The imaginary part becomes deeper with increasing energies and it changes from a slightly surface–peaked shape at 40 MeV (although not very well visible in the scale of Fig. 7) to a center–peaked shape at 105 MeV. These features were also observed in the results of Ref. [23] although, again, we obtain a much shallower depth for the imaginary part of the Λ optical potential. At 40 MeV, for instance, we obtain a depth of about -0.2 MeV while the value obtained in Ref. [23] is -2.4 MeV.

From this analysis we conclude that, in order to derive hypernuclear properties, microscopic calculations of the effective interaction must be combined with a reliable treatment of the finite hypernucleus under consideration since the single–particle Λ properties (single–particle energy, wave functions, optical potential) are sensitive to the particular model. This is especially relevant at present for the analysis of the high resolution hypernuclear spectroscopy experiments which are going to be conducted at CEBAF.

IV. CONCLUSIONS

In this work we have calculated the self–energy of a Λ in the finite nucleus $^{17}_\Lambda$O using a microscopic many–body approach which allows to study the energy dependence as well as the momentum dependence of the self–energy for a finite nucleus, starting with realistic modern potential models for the hyperon–nucleon (YN) interaction. As models for the YN–interaction we have used the meson–exchange models of the Nijmegen [11] and Jülich groups [12]. The Jülich potential yields a more attractive Λ single–particle energy in nuclear matter than the Nijmegen potential. The same qualitative pattern is repeated in the finite nucleus calculation, where the single–particle energy for a Λ in the

$0s_{1/2}$ state in $^{17}_{\Lambda}$O is -11.83 MeV and -7.38 MeV with Jülich and Nijmegen potentials, respectively. The experimental estimate from Ref. [29] is -12.5 MeV. The self–energy is in turn used to derive an optical potential for the Λ–nucleus system. It turns out that the real and imaginary parts of our non-local optical potential can easily be approximated by the shape of a Woods–Saxon potential with a depth depending on energy. This local equivalent potential is less attractive than those derived from the local–density calculation of Ref. [23].

V. ACKNOWLEDGMENTS

[1] M. Juric et al., Nucl. Phys. B52 (1973) 1; M. Cantwell et al., Nucl. Phys. A236 (1974) 445; J. Pniewski et al., Nucl. Phys. A443 (1985) 685.
[2] R. Bertini et al., Phys. Lett. B83 (1979) 306; Nucl. Phys. A360 (1981) 315; A368 (1981) 365.
[3] W. Brückner et al., Phys. Lett. B55 (1975) 107; B62 (1976) 481; B79 (1978) 157.
[4] R.E. Chrien et al., Phys. Lett. B89 (1979) 31; B. Povh, Nucl. Phys. A335 (1980) 233; M. May et al., Phys. Rev. Lett. 47 (1981) 1106.
[5] R.A. Schumacher, Nucl. Phys. A585 (1995) 63c.
[6] R. Engelmann et al., Phys. Lett. 21 (1966) 587.
[7] G. Alexander et al., Phys. Rev. 173 (1968) 1452.
[8] B. Sechi–Zorn et al., Phys. Rev. 175 (1968) 1735.
[9] J.A. Kadyk et al., Nucl. Phys. B27 (1971) 13.
[10] J. Eisele et al., Phys. Lett. B37 (1971) 204.
[11] M.M. Nagels, T.A. Rijken and J.J. de Swart, Phys. Rev. D15, 2547 (1977); P.M.M. Maessen, T.A. Rijken, and J.J. de Swart, Phys. Rev. C40, 2226 (1989).
[12] B. Holzenkamp, K. Holinde, and J. Speth, Nucl. Phys. A500, 485 (1989).
[13] A. Reuber, K. Holinde and J. Speth, Nucl. Phys. A570 (1994) 543.
[14] K. Migayawa and W. Glöckle, Phys. Rev. C48 (1993) 2576.
[15] K. Migayawa, H. Kamada, W. Glöckle and V. Stoks, Phys. Rev. C51 (1995) 2905.
[16] B.F. Gibson and D.R. Lehman, Phys. Rev. C37 (1988) 679.
[17] Y. Yamamoto and H. Bandō, Prog. Theor. Phys. 83 (1990) 254.
[18] Y. Yamamoto, A. Reuber, H. Himeno, S. Nagata and T. Motoba, Czec. Jour. Phys. 42 (1992) 1249; Y. Yamamoto, T. Motoba, H. Himeno, K. Ikeda and S. Nagata, Prog. Theor. Phys. Suppl. 117 (1994) 361.
[19] J. Hao, T.T.S. Kuo, A. Reuber, K. Holinde, J. Speth and D.J. Millener, Phys. Rev. Lett. 71 (1993) 1498.
[20] D. Halderson, Phys. Rev. C48 (1993) 581.
[21] CEBAF experiment 91–014 (C.E. Hyde-Wright spokesperson).
[22] KEK PS–E251 and E289 collaboration. J.K. Ahn et al., Nucl. Phys. A585 (1995) 165c.
[23] Y. Yamamoto and H. Bandō, Phys. Lett. B214 (1988) 173.
[24] E.D. Cooper, B.K. Jennings and J. Mareš, Nucl. Phys. A580 (1994) 419.
[25] M. Borromeo, D. Bonatsos, H. Müther and A. Polls, Nucl. Phys. A539 (1992) 189
[26] M. Hjorth–Jensen, M. Borromeo, H. Müther and A. Polls, Nucl. Phys. A551 (1993) 580
[27] C.L. Kung, T.T.S. Kuo and K.F. Ratcliff, Phys. Rev. C19 (1979) 1063
[28] C.W. Wong and D.M. Clement, Nucl. Phys. A183 (1972) 210
[29] H. Bandō, T. Motoba and J. Žofka, Int. J. Mod. Phys. A5 (1990) 4021.
[30] C. Mahaux and R. Sartor, Adv. in Nucl. Phys. 20 (1991) 1.

TABLE I. Partial wave contributions to the binding energy of the Λ in nuclear matter for the Jülich and Nijmegen potentials at Fermi momentum $k_F = 1.4$ fm^{-1}. Numbers in parentheses refer to the case when the coupling to intermediate ΣN is omitted in the calculation of the ΛN G–matrix. The total numbers include partial waves with total angular momentum $J \leq 4$. All entries in MeV.

	$^1S_0$	$^3S_1-^3D_1$	$^3P_0$	$^1P_1-^3P_1$	$^3P_2-^3F_2$	Total
Jülich	-0.6	-33.95	0.59	3.04	0.093	-31.48
	(1.61)	(-19.98)	(0.62)	(3.31)	(0.25)	(-11.93)
Nijmegen	-14.99	-8.17	0.37	3.54	-3.88	-24.35
	(-13.84)	(13.63)	(0.43)	(4.36)	(-2.92)	(0.57)

TABLE II. Single–particle energy (ε_Λ), mean–square radius (rms) and kinetic energy (T) for a Λ in the $0s_{1/2}$ state of $^{17}_\Lambda$O. The results are given for the Jülich and Nijmegen potentials and for two approximations to the self–energy: the Hartree–Fock (HF) and the Hartree–Fock plus the two–particle–one–hole diagram (HF+2P1H). Energies are in units of MeV and rms in units of fm.

	Jülich		Nijmegen		Exp
	HF	HF+2P1H	HF	HF+2P1H	
ε_Λ	-10.15	-11.83	-4.76	-7.38	-12.5 [29]
T	6.43	6.49	4.43	5.08	
rms	2.49	2.47	3.04	2.80	

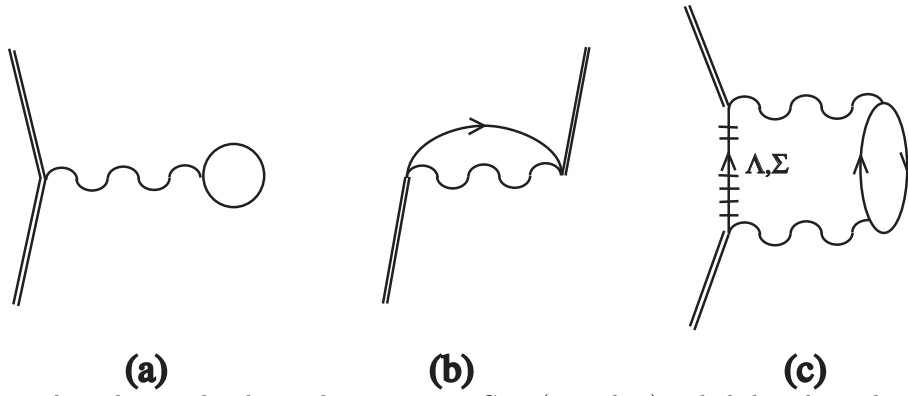**(a)**   **(b)**   **(c)**

FIG. 1. Diagrams through second order in the interaction G_{YN} (wavy line) included in the evaluation of the self–energy of the Λ. Diagrams (a) and (b) represent the direct and the exchange Hartree–Fock terms, while (c) is an example of the second order two–particle–one–hole diagram. Note that the double external lines represent a Λ while the "railed" line in (c) refers to a intermediate Λ and Σ hyperon.
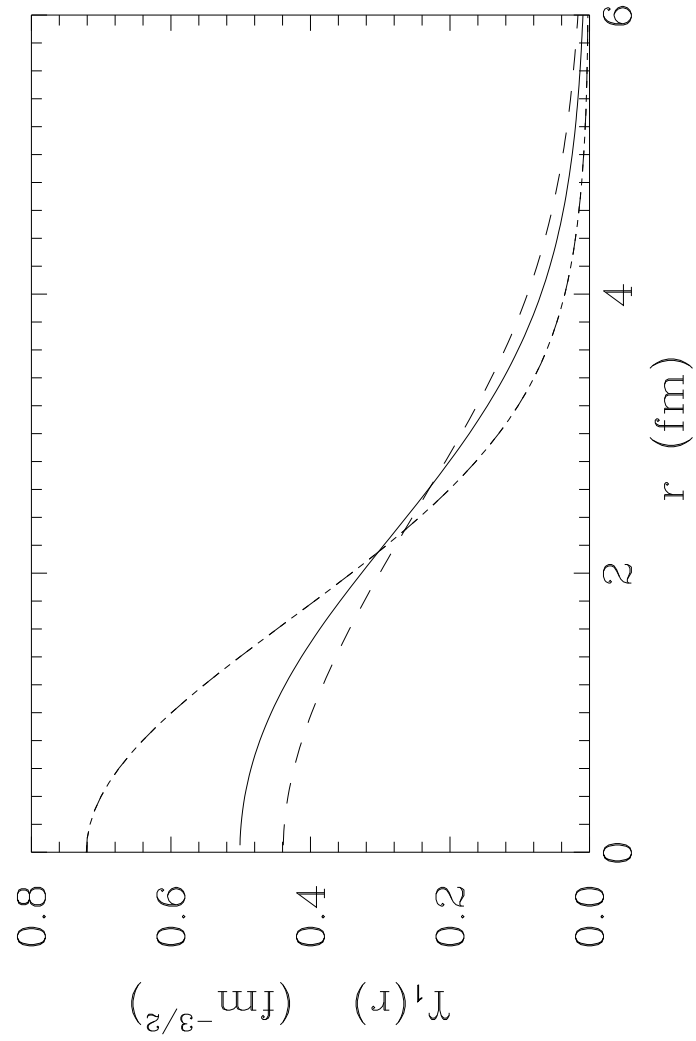
FIG. 2. Wave function in r–space for the Λ in the $0s_{1/2}$ state in $^{17}_{\Lambda}$O for the Jülich (solid line) and the Nijmegen (dashed line) potentials. For comparison we include the single nucleon wave function (dash–dotted line) in ^{16}O from Ref. [26].
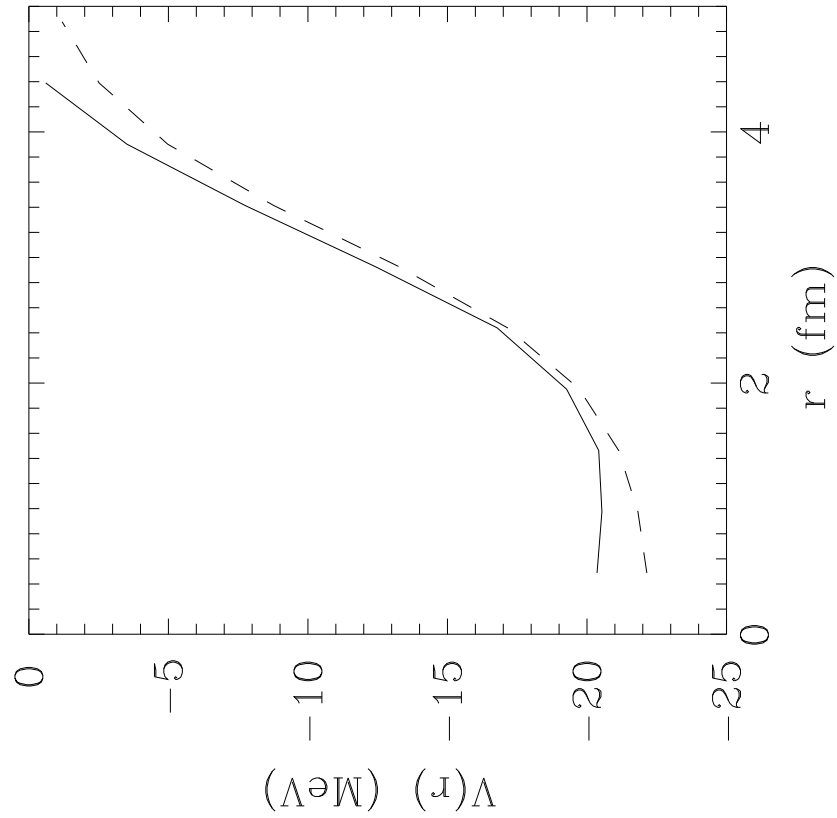
FIG. 3. Local single–particle potentials for a Λ in the $0s_{1/2}$ state in $^{17}_{\Lambda}$O employing the Jülich potential. Solid line represents the results obtained from Eq. (19) while the dashed line is the result obtained with the Woods–Saxon parametrization discussed in the text.
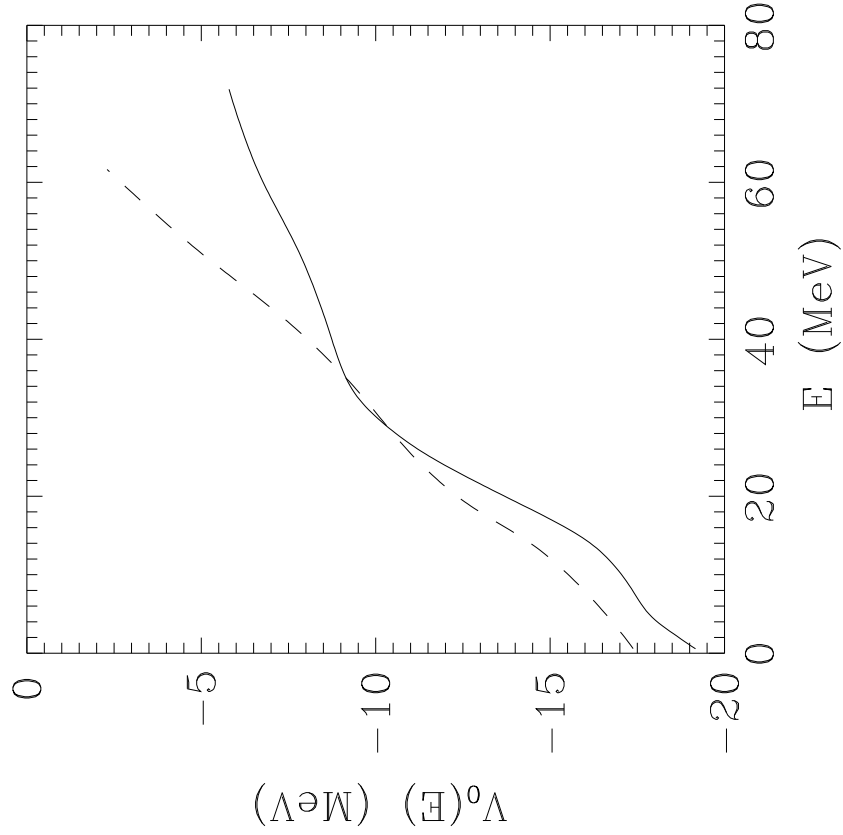
FIG. 4. Energy dependence of the depth of the Λ–nucleus Woods–Saxon potential for a Λ in the $l = 0$ state employing the Jülich potential. The dashed line shows the depths resulting from fitting the phase–shifts to those obtained by including only the Hartree–Fock diagram to the self–energy. Solid line is obtained by including also the two–particle–one–hole diagram in the evaluation of the self–energy.
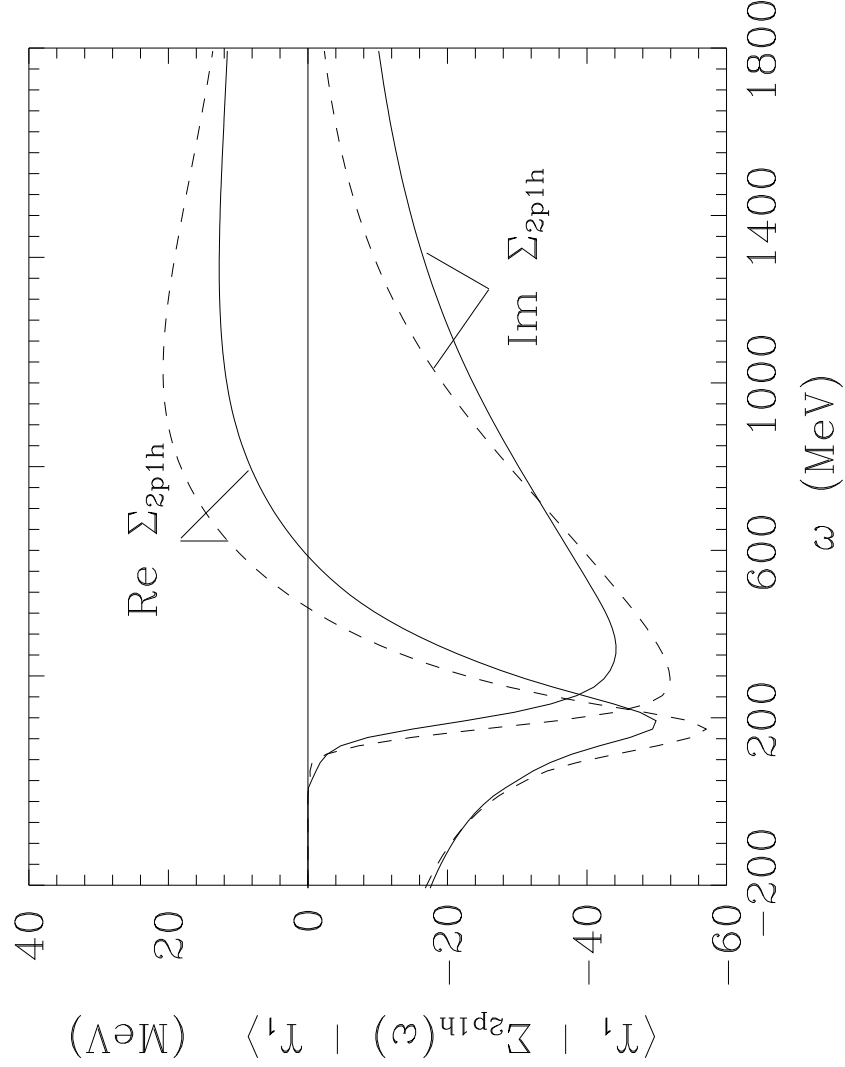
FIG. 5. Ground state expectation value of the real and imaginary parts of the dispersive term of the Λ self–energy as functions of ω. Solid lines are results obtained with the Jülich potential while dashed lines are those of the Nijmegen potential.
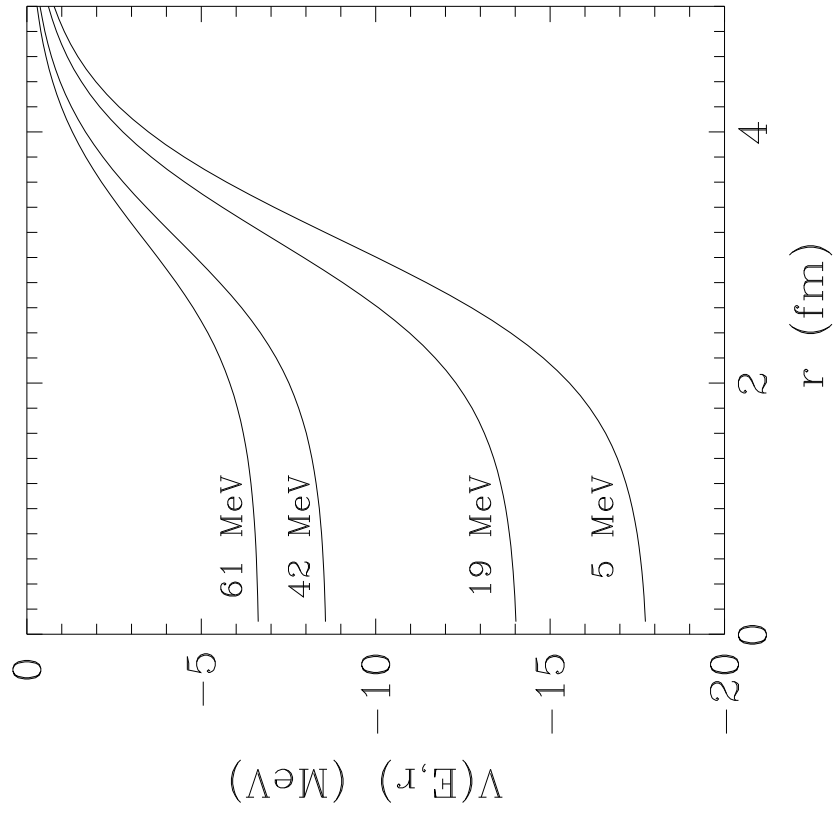
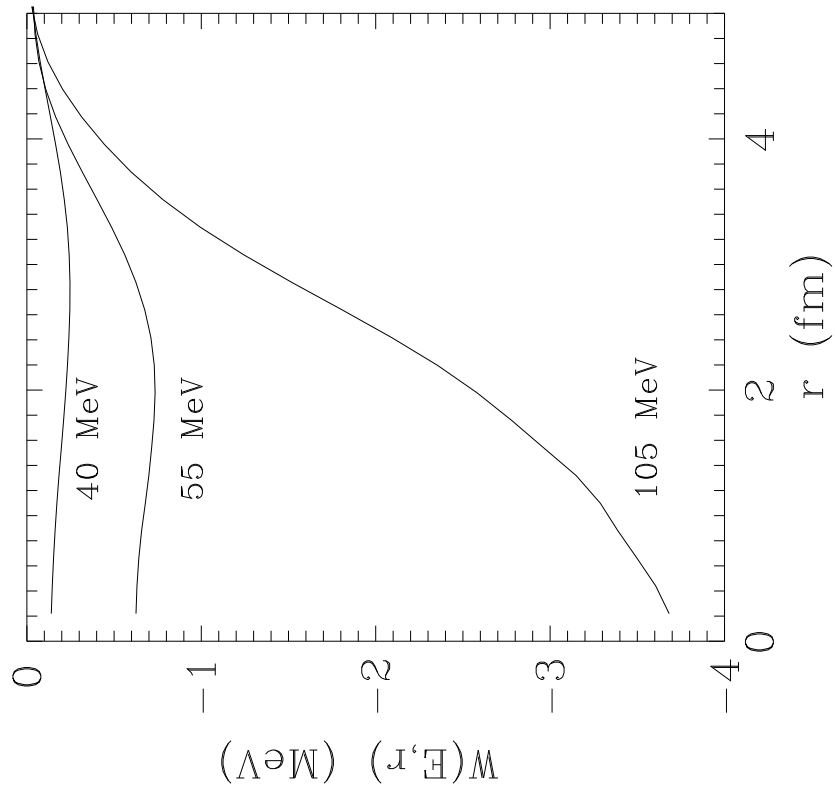FIG. 6. Local Λ–nucleus Woods–Saxon potential at different Λ energies for a Λ in the $l = 0$ state.

FIG. 7. Imaginary part of the optical potential at different Λ energies for a Λ in the $l = 0$ state.